  Bull. Chem. Soc. Jpn., 64, 3700—3706 (1991) [Vol. 64, No. 12

On the Splittings of J-Aggregate Band in Pseudoisocyanine

Hirotoshi Ito,* Masaru Agatsuma, and Y. J. I'Haya
Department of Applied Physics and Chemistry, The University of Electro-Communications, 1-5-1, Chofugaoka, Chofu, Tokyo 182
(Received June 3, 1991)

The observation of J-band splittings in the Fano–DeVoe type calculations of pseudoisocyanine aggregates is reported. Based upon the monoclinic structure of pseudoisocyanine iodide crystal, we build four models which respectively assume the lattice constants of the crystal structure. The one-dimensional (1D-) single polymer model is selected along a particular direction from the crystal structure. As we diminish the lattice constants uniformly, the 1D-single-polymer model comes to reproduce single J-bands, while two kinds of 2D-two-inter-polymer interaction models resolve the single J-bands into doublet through multiplet structures for the corresponding parameters. The 3D-four-inter-polymer interaction model brings about doubly split J-bands, but the shortening of the parameters resolves the doublet J-bands into quartet through multiplet structures. However, a single J-band is obtained by the assumption of an orthorhombic 3D-four-inter-polymer model which has the same parameters as those of the monoclinic iodide crystal except for the angle. The shapes calculated are found to be extremely sensitive to the geometrical values as well as the monomer spectroscopic parameters. The cause of the J-band splittings is ascribable to the excitonic interactions between at least two column polymers.

Aqueous solutions of pseudoisocyanine dyes (1,1′-diethyl-2,2′-cyanine, PIC dyes) at high concentrations show extraordinarily narrow, intense *single* bands.[1,2] Similar kinds of bands observed in various cyanine dye aggregates are called J-bands after the discover Jelley,[1] and such aggregates are called J-aggregates or sometimes Scheibe-aggregates. Cooper[3,4] first observed that in a transparent ethylene glycol–water (EGW) matrix at 77 K, such a single J-band of PIC bromide is split into two extremely sharp bands of almost equal intensity separated by 151 cm^{-1}. Also in EGW solution at 77 K, a weak doublet structure of the J-band of PIC iodide was found by Tanaka et al.[5] as a shoulder at shorter wavelength side of the main peak. Perhaps due to the excess amount of iodide ions,[5] Marchetti et al.[6] did not observe the split J-band of PIC iodide in the same EGW solution with 0.1 M KI at 77 K (1 M=1 mol dm^{-3}). Furthermore, Yu et al.[8] observed that the intensities of split J-spectra of PIC bromide in EGW solution become stronger gradually as temperature is reduced below 210 K down to 80 K. It has recently been reported that the relative intensity of split J-bands of PIC bromide changes with the cooling procedure of the glassy solution.[9,10] However also in Ref. 10, Murata has found that the peak appeared at shorter wavelength side of the single J-band of PIC iodide is always weaker than the peak appeared at longer wavelength side, as was reported before.[5] These phenomena lends qualitative supports for the present assumption that J-aggregate models in solutions are similar to the structures of microcrystals of PIC halides.

Any theoretical work has not been done to elucidate the cause of J-band splittings. Cooper[3,4] suggested that the split J-transitions are assigned to two energy levels respectively for the mixed J_1 and J_2 aggregates consisting two different configurations of PIC dye to the axis of PIC polymer chosen in a particular direction. However, he also referred to the excitonic nature of the split J-band, and from Refs. 3 and 4, we cannot deny in a broad meaning such a scheme that the coupling between at least two linear (1D-) J-aggregates of different geometrical orientations gives rise to Davydov splitting.

Our calculations to elucidate this are based upon the Fano–DeVoe theory and its versions,[11—16] which have provided an excellent tool for predicting bandshapes of various polymer systems. First, Briggs and Herzenberg[13,14] beautifully predicted the *single* J-bandshape for the most simplified PIC aggregate model in terms of their coherent exciton scattering theory equivalent to the Fano–DeVoe one. Also, Sumi[15] carried out a coherent potential approximation (CPA) calculation, which gives a single J-like band. Later on, to a rather real model than before, Knapp et al.[16] have applied a simplified version of the CPA theory.[15] They have been able to reproduce a single J-band for the cyclic 1D-aggregate model consisting of 11 PIC molecules by making use of model parameters determined for the PIC monomer and dimer spectra.[17] This treatment is based upon the assumption that the structure of dimer is almost similar to those of dimer units in the longer as well as wider spread J-aggregates. Scherer and Fischer[18] have also followed this treatment for the linear J-aggregates. Thus in their calculations, equi-magnitudes of inter-(sub)molecular interactions have been taken into account as geometrical factors. However, the interaction potentials of J-aggregates are supposed to be not only of short-range forces, but also of long-range forces. Tanaka et al.[5] suggested that such interactions have highly direction dependences for specific neighboring PIC molecules, that is, such interactions are highly anisotropic. Therefore first of all, for a better understanding of J-bands, it is important and necessary to take into account the *explicit geometries* of models which are derived from the crystal structure of the PIC molecule,[29] so that we can involve all the possible

inter(sub)molecular interactions.

Polymer Polarizability Tensor

The *extended* Fano–DeVoe model Hamiltonian of the polymer (N-mer) is assumed to be[19]

$$H=\sum_{f}^{\text{levels}}\sum_{m}^{N}\sum_{g}^{\text{levels}}\sum_{n}^{N}|\psi_m^f\prod_{k\neq m}^{N}\psi_k^0\rangle\langle\psi_m^f\prod_{k\neq m}^{N}\psi_k^0|\,\mathcal{H}|\psi_n^g\prod_{k\neq n}^{N}\psi_k^0\rangle\langle\psi_n^g\prod_{k\neq n}^{N}\psi_k^0|$$
$$-\langle\prod_{k=1}^{N}\psi_k^0|\,\mathcal{H}|\prod_{k=1}^{N}\psi_k^0\rangle\equiv\sum_{f,g}^{\text{levels}}\sum_{m,n}^{\text{sites}}|fm\rangle\langle fm|\,\mathcal{H}|gn\rangle\langle gn|$$
$$-\langle 0|\,\mathcal{H}|\,0\rangle$$
$$=\sum_{f\neq 0}^{\text{level}}\sum_{m}^{\text{sites}}E_{fm,0}|fm\rangle\langle fm|+\sum_{f,g\neq 0}^{\text{levels}}\sum_{m,n}^{\text{sites}}|fm\rangle\langle fm|\mathcal{V}_{mn}|gn\rangle\langle gn|$$
$$\equiv H_0+V, \tag{1}$$

with

$$\mathcal{H}=\sum_{m=0}^{\text{sites}}\mathcal{H}_m^0+\sum_{m>n}^{\text{sites}}\sum^{\text{sites}}\mathcal{V}_{mn},\qquad(\mathcal{V}_{mn}\approx\boldsymbol{\mu}_m\cdot\boldsymbol{U}_{mn}\cdot\boldsymbol{\mu}_n) \tag{2}$$

and with the unit dipole–dipole interaction tensor

$$\boldsymbol{U}_{mn}=\frac{1}{|\boldsymbol{R}_{mn}|^5}\{|\boldsymbol{R}_{mn}|^2\mathbb{1}-3\,\boldsymbol{R}_{mn}\boldsymbol{R}_{mn}\},\qquad\boldsymbol{R}_{mn}=\boldsymbol{R}_n-\boldsymbol{R}_m. \tag{3}$$

In the present calculations however, the lowest excited level only is taken into account for simplicity, so that we put actually $f=g$ in the second term of Eq. 1. Note that for the *original* Fano–DeVoe approximation, we must drop the electrostatic term $\langle fm|V|gm\rangle$ involved in Eq. 1. In Eqs. 1 and 2, $\mathcal{H}_m^0$ is the electronic Hamiltonian for the mth submolecule, $\mathcal{V}_{mn}$ the inter(sub)molecular interaction operator, and $\boldsymbol{\mu}_m$ the mth electric dipole moment operator. The eigen-functions ψ_m^0 *and* ψ_m^f for the monomer Hamiltonian $\mathcal{H}_m^0$, respectively, denote the *ground* and the fth *locally excited* states associated with the eigen-values E_0^m and E_f^m, their difference being put to be $E_{fm,0}$. For simplicity, we do not consider the electrostatic shift of $E_{fm,0}$ due to neighboring PIC cations and their counter anions, although we can theoretically make an allowance for such effects, for instance on the basis of Refs. 17—19 and Ref. 24. In Eq. 3, we assume the validity of the dipole–dipole approximation, since it was shown by Tanaka et al.[5] that the distances of neighboring molecules in PIC crystals are larger than the overlapping size of pi-electron clouds from the calculations of overlap integrals.

For the *crude* and *true* Green's operators G_o(E) and $G(E)$ defined by Eq. 1, we have the sum of the mth monomer polarizability tensor $\boldsymbol{\alpha}_{mm}(E)$

$$-\langle 0|\boldsymbol{\mu}G_o(E)\boldsymbol{\mu}|0\rangle=-\langle|\boldsymbol{\mu}(E-H_o+i\eta)^{-1}\boldsymbol{\mu}|0\rangle$$
$$=-\sum_{m}^{N}\sum_{f\neq 0}^{\text{levels}}\frac{\boldsymbol{\mu}_{0f}^{(m)}\boldsymbol{\mu}_{f0}^{(m)}}{E-E_{fm,0}+i\eta_{fm}}\equiv\sum_{m}^{N}\boldsymbol{\alpha}_{mm}(E), \tag{4}$$

where the matrix element of the total electric dipole operator is given by

$$\boldsymbol{\mu}_{0f}^{(m)}=\langle 0|\boldsymbol{\mu}|fm\rangle\equiv\langle 0|\sum_{m}^{N}\boldsymbol{\mu}_m|fm\rangle$$
$$=\langle 0|\sum_{m}^{N}\{\sum_{i\in m}^{\text{elec}}e\boldsymbol{r}_{mi}-\sum_{J\in m}^{\text{nuc}}eZ_J\boldsymbol{r}_{mJ}\}|fm\rangle,\qquad(\boldsymbol{r}_{mi}=\boldsymbol{r}_i-\boldsymbol{r}_m) \tag{5}$$

The m,n-element of the polymer polarizability tensor ${}^p\boldsymbol{\alpha}_{mn}(E)$ is then reduced to

$$-\langle 0|\boldsymbol{\mu}G(E)\boldsymbol{\mu}|0\rangle=-\langle 0|\boldsymbol{\mu}(E-H+i\eta)^{-1}\boldsymbol{\mu}|0\rangle$$
$$=-\langle 0|\boldsymbol{\mu}\{G_o(E)+G_o(E)VG_o(E)+\cdots\}\boldsymbol{\mu}|0\rangle$$
$$\equiv\sum_{m=1}^{N}\sum_{n=1}^{N}{}^p\boldsymbol{\alpha}_{mn}(E) \tag{6}$$

Inserting the resolution of identities ($\sum\sum|fm\rangle\langle fm|=1$) with use of the relationships such as $\langle fm|\mathcal{V}_{mn}|gn\rangle\approx\boldsymbol{\mu}_{f0}^{(m)}\cdot\boldsymbol{U}_{mn}\cdot\boldsymbol{\mu}_{0g}^{(n)}$, we can derive

$${}^p\boldsymbol{\alpha}_{mn}(E)=\{\mathbb{1}+\mathfrak{A}(E)\cdot\mathbb{U}\}_{mn}^{-1}\cdot\boldsymbol{\alpha}_{nn}(E),\qquad m,n=1,2....,N \tag{7}$$

where the suffices m,n of $\mathbb{1}$, $\mathfrak{A}(E)$, and $\mathbb{U}$ denote the elements of the corresponding $3N\times 3N$ matrices.

Vibronic Description of Monomer Polarizability Tensor

The purely electronic scheme in the previous section can be extended to the vibronic problem. In the adiabatic approximation, the ground and fth excited states of the mth monomer appearing in Eq. 1 are replaced by the products:

$$\psi_m^f\rightarrow\psi_m^f(\boldsymbol{r},\boldsymbol{Q})\chi_m^{f,v}(\boldsymbol{Q})=\psi_m^f(\boldsymbol{r},\boldsymbol{Q})\prod_{k}^{3N-6}X_{m^k}^{f,v_k}(\boldsymbol{Q}_k),\qquad(f=0,f) \tag{8}$$

where the $\boldsymbol{r},\boldsymbol{Q}$ represent collective coordinates for electrons and nuclei. $\chi_m^{f,v}$ represents the total vibrational eigenstate associated with the eigenvalue $E_{f,v}^{m,\text{vib}}$, where v denotes a set of vibrational quantum numbers, i.e., $v\equiv(v_1,v_2,v_3,\cdots v_k\cdots v_{3N-6})$ for the $3N-6$ harmonic-oscillator wavefunctions. In the adiabatic approximation, the mth monomer Hamiltonian for the fixed nuclei is expressed by

$$H_m^0=\sum_{f=f,0}^{\text{levels}}E_f^m(\boldsymbol{Q})|\psi_m^f(\boldsymbol{r},\boldsymbol{Q})\rangle\langle\psi_m^f(\boldsymbol{r},\boldsymbol{Q})|.\qquad(\text{in }H^0=\sum_{m}^{\text{sites}}H_m^0) \tag{9}$$

Now, $E_f^m(\boldsymbol{Q})$ becomes the effective adiabatic potential for the nuclear motion. The nonadiabatic (NA) Hamiltonian of the mth monomer is then represented by

$$H_m^0\rightarrow H_m^0=\sum_{f=f,0}\sum_{v}(E_f^m+E_{f,v}^{m,\text{vib}})|\psi_m^f\rangle|\chi_m^{f,v}\rangle\langle\chi_m^{f,v}|\langle\psi_m^f|$$
$$+\sum_{f\neq g}\sum\sum_{v}\sum_{v'}\sum_{k}^{\text{vib. mode}}|\psi_m^f\rangle|\chi_m^{f,v}\rangle\mathcal{V}_{m,\text{NA}}^{(f,k,g)}\langle\chi_m^{g,v}|\langle\psi_m^g|, \tag{10}$$

where the off-diagonal term is the *intra*(sub)molecular vibronic coupling (NA) operator.[22] However, to simplify the problem, we do not take such a coupling operator into account. After all, modification of Eq. 1 in terms of Eq. 8 needs the replacement of $E_{fm,0}$ with $E_{\text{fm},0}^{(v)}$ that denotes the vth vibrational state on the fth electronic excited state of an mth monomer. Namely, a vibronically excited level relative to the zero-temperature ground state, leaving the other vibrational

states in the ground state, is written down

$$E_{fm,0} \rightarrow E^{(v)}_{fm,0} = E_{fm,0} + [E_{fm,v} - E_{0m,0}] \equiv E_{fm,0} + E_{fm,0;v0}$$
$$= E_{fm,0} + vE_{fm,0;10} = hc\tilde{\nu}^{(v)}_{fm,0} = h\nu(\tilde{\nu}_{fm,0} + v\,\tilde{\nu}_{fm,0;10}), \quad (11)$$

where $E_{fm,0;10}$ becomes a fundamental vibrational energy on the fth electronic level. The purely electronic transition moment $\boldsymbol{\mu}^{(m)}_{0f}$ is also replaced with the vibronic moment multiplied by the Franck–Condon overlap integral, so that the inter(sub)molecular interaction becomes

$$<fm|\mathcal{V}_{mn}|gn> \approx \boldsymbol{\mu}^{(m)}_{f0} \cdot \boldsymbol{U}_{mn} \cdot \boldsymbol{\mu}^{(n)}_{0g}$$
$$\rightarrow \boldsymbol{\mu}^{(m)}_{0f} <\chi^{0,0}_m|\chi^{f,\nu}_m> \cdot \boldsymbol{U}_{mn} \cdot \boldsymbol{\mu}^{(n)}_{0g} <\chi^{0,0}_n|\chi^{g,\nu'}_n>. \quad (12)$$

The imaginary part of the usual type of monomer polarizability tensor(in units of cm^3) is given by

$$\mathrm{Im}\ \boldsymbol{\alpha}_{nn}(\tilde{\nu}) = \sum_{g\neq 0}\sum_{\nu} \frac{+e^2}{hc} \{\boldsymbol{\mu}^{(n)}_{0g}/e\}\{\boldsymbol{\mu}^{(n)}_{g0}/e\} \times$$
$$|<\chi^{0,0}_n|\chi^{g,\nu}_n>|^2 \pi\delta[\tilde{\nu} - \tilde{\nu}^{(\nu)}_{gn,0}], \quad (e^2/hc = 1.16138\times 10^{-3}), \quad (13)$$

which corresponds to the treatment made by Hemenger.[23] Actually, the lowest excited sate alone is taken into account for the gth states in Eq. 13, so that we put $f=g$ in Eq. 12.

The δ function in Fq. 13 are usually approximated by both the *Gaussian* and *Lorentzian* type functions. By many investigators,[13,14,16,20] it has been revealed that use of Gaussian type monomer functions can predict J-bands, whichever monomer function we may choose of vibronic and purely electronic polarizabilities. However, Lorentzian type functions were found to require the *vibronic* type monomer polarizability in order to reproduce J-bands.[20,21] We also replace Eq. 13 by the Gaussian function as follows:

$$\mathrm{Im}\ \boldsymbol{\alpha}_{nn}(\tilde{\nu}) = \sum_{g\neq 0}\sum_{\nu} \frac{+e^2}{hc} \{\boldsymbol{\mu}^{(n)}_{0g}/e\}\{\boldsymbol{\mu}^{(n)}_{g0}/e\}|<\chi^{0,0}_n|\chi^{g,\nu}_n>|^2 \times$$
$$\left(\frac{\sqrt{\pi}}{\tilde{\Delta}^{(\nu)}_{gn}}\right)\exp\left\{-\left(\frac{\tilde{\nu} - \tilde{\nu}^{(\nu)}_{gn,0}}{\tilde{\Delta}^{(\nu)}_{gn}}\right)^2\right\} \equiv \sum_{g\neq 0}\sum_{\nu} \mathrm{F}[(\tilde{\nu} - \tilde{\nu}^{(\nu)}_{gn,0})/\tilde{\Delta}^{(\nu)}_{gn}], \quad (14)$$

where the bandwidth (FWHM in cm^{-1}) has a relationship such as $\tilde{\Gamma}^{(\nu)}_{gn} = 2\sqrt{\ln 2}\,\tilde{\Delta}^{(\nu)}_{gn}$ for the normalized Gaussian, and $\tilde{\Delta}^{(\nu)}_{gn}$ is the half-width at $1/e$ of the peak. Then, we determine the magnitude of $\tilde{\Gamma}^{(\nu)}_{gn}$ related with $\tilde{\Delta}^{(\nu)}_{gn}$ so as to adjust $\tilde{\Gamma}^{(\nu)}_{gn}$ to the observed monomer bandshape, i.e., so as to satisfy the following relationship,[24]

$$f_{gn} = 4.59663\times 10^{-9} \sum_{\nu}^{\mathrm{M}} \varepsilon(\tilde{\nu}^{(\nu)}_{gn,0})\,\tilde{\Gamma}^{(\nu)}_{gn}, \quad (15)$$

where we assume the *same* bandwidth for each vibrational peak. Thus using the observed oscillator strength[6] and the corresponding molar extinction coefficient[30] in Eq. 15, the FWHM for the vth vibrational level on the gth (=lowest) electronic level is calculated to be $\tilde{\Gamma}^{(\nu)}_{gn} = 1119.7$ cm^{-1}. In Eq. 11, the values $\tilde{\nu}_{gn,0} = 1915$ cm^{-1} and $\tilde{\nu}^{(\nu)}_{gn,0;10} = 1368$ cm^{-1} are chosen for the *three* vibrational levels (v=0,1,2) on the gth electronic level from Ref. 17. For the Franck–Condon factor, we assume Poisson's distribution,[14,17]

$$|<\chi^{0,0}_n|\chi^{g,\nu}_n>|^2 = \exp(-a^2/2)\frac{(a^2/2)^v}{v!}, \quad (a=1.2) \quad (16)$$

where an adjustable parameter a=1.2 well reproduces the monomer bandshape.

The Kronig–Kramers transform of Eq. 14 gives rise to its real part:[26]

$$\mathrm{Re}\ \boldsymbol{\alpha}_{nn}(\tilde{\nu}) \sum_{g\neq 0}\sum_{\nu} \frac{P}{\pi}\int_{-\infty}^{\infty} \mathrm{d}X \frac{F(X)}{X - (\tilde{\nu} - \tilde{\nu}^{(\nu)}_{gn,0})/\tilde{\Delta}^{(\nu)}_{gn}}$$
$$= \sum_{g\neq 0}\sum_{\nu} \frac{P}{\pi}\int_{-\infty}^{\infty} \mathrm{d}X \frac{\mathrm{Im}\ \boldsymbol{\alpha}_{nn}(\tilde{\nu})}{X - (\tilde{\nu} - \tilde{\nu}^{(\nu)}_{gn,0})/\tilde{\Delta}^{(\nu)}_{gn}}$$
$$= \sum_{g\neq 0}\sum_{\nu} \frac{+e^2}{hc} \{\boldsymbol{\mu}^{(n)}_{0g}/e\}\{\boldsymbol{\mu}^{(n)}_{g0}/e\}|<\chi^{0,0}_n|\chi^{g,\nu}_n>|^2$$
$$\times\left(\frac{2}{\sqrt{\pi}}\right)\left(\frac{\sqrt{\pi}}{\tilde{\Delta}^{(\nu)}_{gn}}\right)\exp\{-[(\tilde{\nu} - \tilde{\nu}^{(\nu)}_{gn,0})/\tilde{\Delta}^{(\nu)}_{gn}]^2\}$$
$$\times\int_0^{(\tilde{\nu}^{(\nu)}_{gn,0} - \tilde{\nu})/\tilde{\Delta}^{(\nu)}_{gn}} \exp(X^2)\mathrm{d}X, \quad (17)$$

which we have numerically calculated. We must report that instead of Eq. 17, use of the simple formula of asymptotic function[24,26] derived from Eq. 17 has not reproduced the J-band.

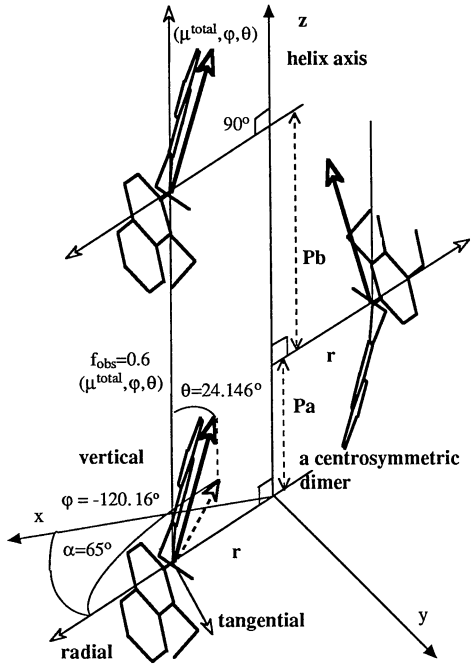

Fig. 1. Schematic illustrations of a quasi 1D-J-aggregate model of PIC which consists of centrosymmetric dimer pairs of PIC's, whose structure is the same as the columns shown on the bottom of Fig. 2. The definitions of the parameter *Pa, Pb,* α, *r,* μ, φ, and θ are given. The direction of the transition moment μ is defined by the angle φ and θ which have been calculated by the CNDO/S method in the Cartesian coordinates used here. We use α=−65.24°, θ=−120.16°, φ=24.16°.

Polymer Bandshape Function J-Aggregate Models

The molar extinction coefficient of the electronic absorption of a polymer system per monomer unit is calculated by

$$^{p}\varepsilon(\tilde{\nu}) = (8\pi^2 N_A/2301.6)\tilde{\nu}\frac{1}{N}\sum_{m}^{N}\sum_{n}^{N}\mathrm{Im}\left[\frac{1}{3}\mathrm{Tr}\,{}^{p}\boldsymbol{\alpha}_{mn}(\tilde{\nu})\right], \quad (1\ \mathrm{mol}^{-1}\,\mathrm{cm}^{-1}). \quad (18)$$

In Fig. 1, we give schematic illustrations of 1D-J-aggregate model with defintion of parameters. The model consists of a helical array of the transition moments $\boldsymbol{\mu}_{g0}^{(n)}$ of propeller-like molecule PIC. As mentioned before, the magnitudes of $|\boldsymbol{\mu}_{g0}^{(n)}|$, $\tilde{I}_{gn}^{(v)}$ and $\tilde{\Delta}_{gn}^{(v)}$ are estimated from the observed oscillator strength f_{gn}=0.6[6] and its molar extinction coefficient.[30] However, we have no knowledge about the direction of the transition moment. So on the bottom in Fig. 1, we have shown the results of CI calculation of the direction (φ=24.146° and θ=−120.16°) of the total transition moment $\boldsymbol{\mu}_{g0}^{(n)}$ of the lowest electronic excited level for the Cartesian coordinate system given here. Clearly, the transition has the ππ*-character. The 40×40 singly excited CI calculation, whose configurations are chosen from the 8 higher occupied MO's involving HOMO and the 5 low-lying vacant MO's involving LUMO, has been carried out by the CNDO/S method[31] using the geometry of PIC chloride.[27] Also, other X-ray data of PIC halides gave almost similar results. The values of $\tilde{\nu}_{gn,0}$ and f_{gn} for the lowest level are respectively calculated to be 19544 cm^{-1} and 1.07, which are compared with the observed values 19150 cm^{-1} and 0.6. Similarities of J-aggregate models in solutions to the microcrystals of PIC halides were discussed by several authors.[6,29,30] In Fig. 2, we depict a rather simplified 3D-column model picked out along the[101]-direction from the crystal structure of PIC iodide reported by Nakatsu et al.[29] They indicated that the crystal structure is similar to the stair case orientation of dyes of the slipped-deck-of-card type[33] and also to the A1 of the brickstone model.[30] In Fig. 2, each column consists of quasi-1D-sequences of centrosymmetric dimer pairs, so that each column (A,B,A′,B′) constitutes the 1D-polymer model (*1D-J-aggregate*) for which we here assume 10-mer. *Two*-column interactions between A and A′ and/or between B and B′ define the 2D-polymer model (*2D-J1-aggregate*), while *two*-column interactions between A and B and/or between A′ and B constitute the 2D-polymer model (*2D-J2-aggregate*) which is slightly different from the 2D-J1-aggregate model. Here, we do not consider 2D-polymer models such as (A,B′) as well as (A′,B) models. The 3D-polymer model (*3D-J-aggregate*) is defined from *four*-column interactions among A,B,A′, and B′.

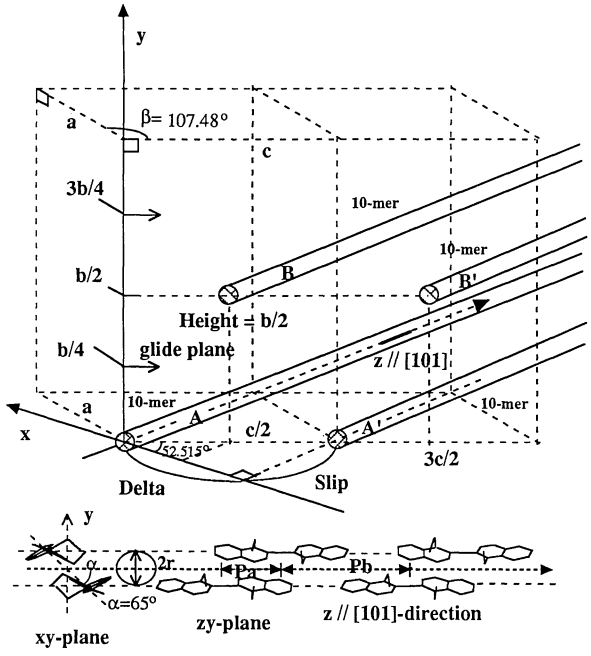

Fig. 2. The 3D-continuation of columns consisting of quasi-1D sequence of centrosymmetric dimer pairs,[29] which are produced by the operations of the *c* glide planes and specified with three parameters such as Delta, Slip, and Height. Each column contains the polymer of PIC's as shown on the bottom. As mentioned in the text, we can defined *four* J-aggregate models such as 1D-J-aggregate, 2D-J1-aggregate, 2D-J2-aggregate, and 3D-J-aggregate.

Results and Discussion

In the calculations, we plot the absorptions of PIC aggregates in the ordinate against the wavelengths with the increment 0.5 nm in the abscissa. In Eq. 18, the summation over large number N is expected to give sufficiently good convergence of bandshapes for any model, but for the 1D-J-aggregate model, all the inter-(sub)molecular interactions between 10-mer give a good convergence. It becomes another reasonable criterion for justifying the 10-mer unit model the fact that the aggregate size of our 10-mer falls into the range within such a molecular size (the values 120 Å $\leqslant$length $\leqslant$500 Å) estimated by Kuhn's energy transfer model of a 1D J-aggregate,[34] so that the range of interactions to be considered may be sufficient. Consequently, the results obtained by considering sufficient chain length effect may be not so different from the present results. In Eqs. 14 and 17, we only take the lowest level over the index g. We have not introduced an isotropic dielectric constant for Eq. 3, although it has often been introduced. This is simply because the introduction of this parameter leads to totally different features of bandshapes for the PIC aggregates. For instance, when we introduce the isotropic dielectric constant 2.0 which is often used in DNA's systems,[12,24] we need to diminish the mutual distances of PIC molecules inappropriately in more compact forms than in the present J-aggregate models in order for reproducing J-bandshapes.

In order to show the dependence of the aggregate

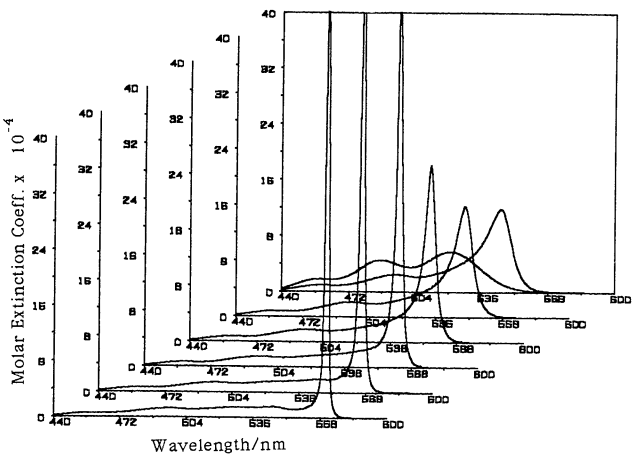

Fig. 3. The absorption spectra for 1D-J-aggregates (*1D-10-mer*). In the L-shaped frames from the left-side to the right-side, each bandshape plotted is calculated by uniformly shortening the parameter (Pa, Pb, Delta, and Slip) of the 1D-J-aggregate crystal model, respectively by the factor 0.6, 0.65, 0.7, 0.8, 0.9, 1.0, but with making the radius r=2.136 Å be constant. In the unscaled model made from Nakatsu's crystal data, we put a=10.787, b=11.626, c=16.484 Å, Pa=8.386 Å, Pb=1.093 Pa, Delta=10.028 Å, Slip=13.080 Å, Height=$b/2$ in Fig. 2. In the most backward frame, the approximate monomer band is plotted.

models upon their geometries, the bandshapes are plotted in Fig. 3 for the small changes of the 1D-J-aggregate crystal model (*1D-10-mer*). Namely, each band shown is calculated by uniformly shortening the lattice constants a, b, c as well as related parameters (Pa, Pb, Slip, and Delta) of the PIC iodide crystal,[29] respectively by the factor 0.6, 0.65, 0.7, 0.8, 0.9, 1.0, but with making the radius r=2.136 Å be constant. These scalings of geometrical parameters are based merely upon the assumption that the structures of J-aggregates in liquids are given by small modifications of PIC crystal structures. The observed peak position 571 nm of the J-band is reproduced by the scaling factor 0.65, while the unsealed 1D-J-aggregate model does show a sharp J-band.

In the *first four* frames of Fig. 4 from the forward one, each bandshape given is calculated respectively by uniformly scaling down the 2D-J2-aggregate crystal model (*2D-20-mer*) by the factor 0.6, 0.7, 0.8, 0.9, and further in the *last four* frames of Fig. 4, each bandshape is respectively plotted by scaling down the 2D-J1 aggregate crystal model (*2D-20-mer*) by the factor 0.6, 0.7, 0.8, 0.9.

In the first four frames of Fig. 5, we plot bandshapes for the 3D-J-aggregate crystal model (*3D-40-mer*), each of which is calculated respectively by uniformly shorten-

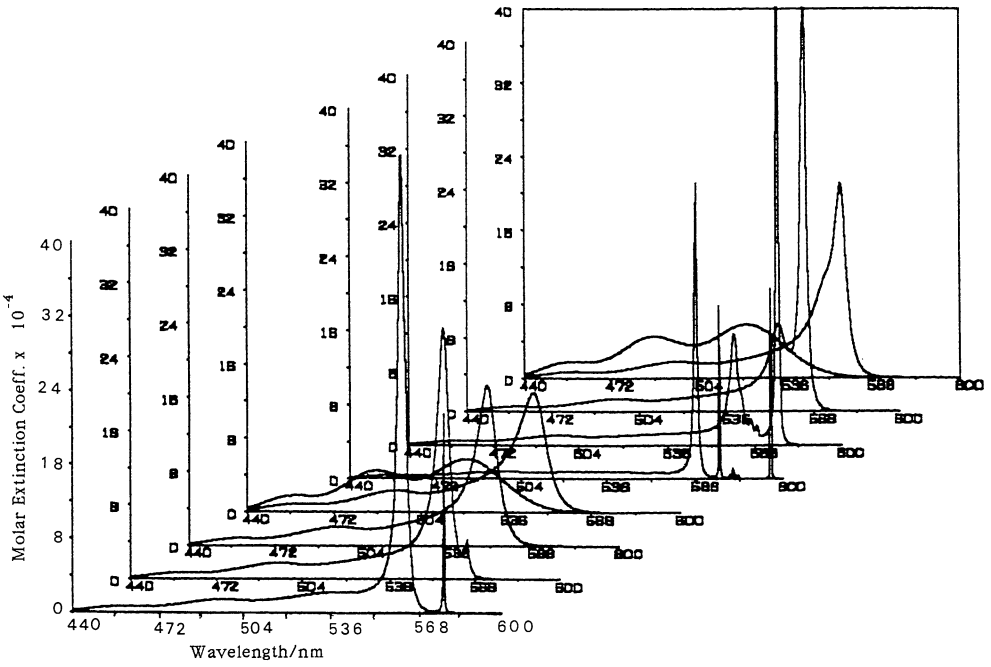

Fig. 4. The absorption spectra for the 2D-J1- and 2D-J2-aggregates. In the L-shaped frames from the left-side to the right-side, each bandshape plotted is calculated by uniformly scaling down the lattice constant (*a, b, c*) as well as the related parameters (*Pa, Pb,* Delta, and Slip) of the 2D-J2-aggregate crystal mode (*2P-20-mer*) respectively by the factor 0.6, 0.7, 0.8, 0.9, and also by uniformly scaling down the 2D-J1-aggregate crystal model (*2D-20-mer*) respectively by the factor 0.6, 0.7, 0.8, 0.9, but with making the radius r=2.136 Å be constant for the both cases. All the parameters used for the unscaled model are the same as those used in Fig. 3.

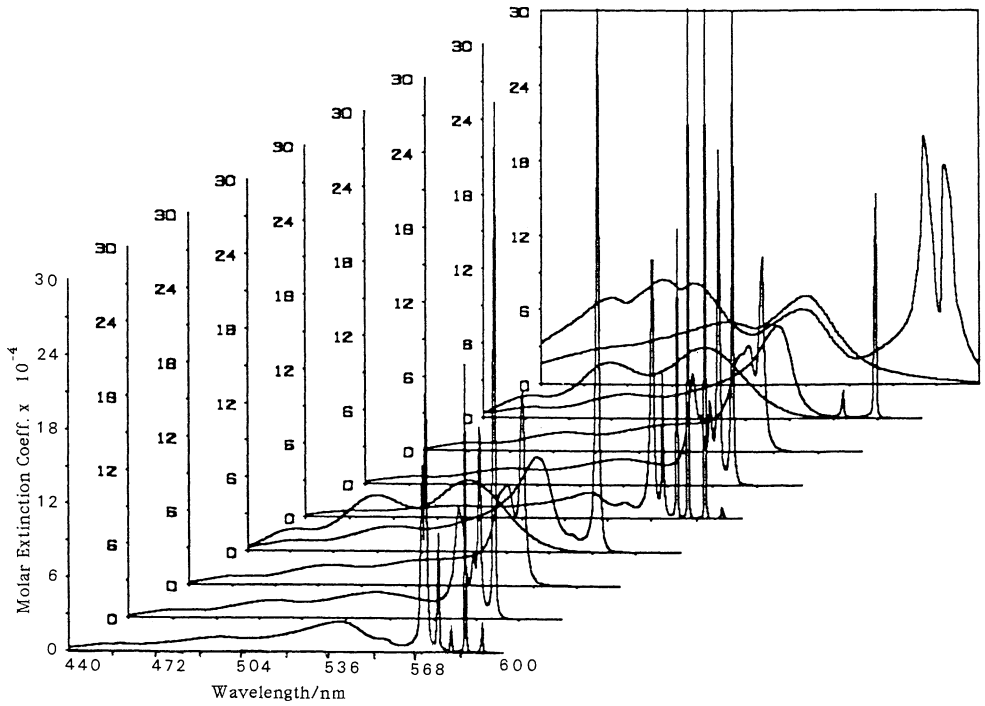

Fig. 5. The absorption spectra for the 3D-J-aggregates. In the *first four* frames, each bandshape shown is calculated by uniformly shortening, respectively by the factor 0.6, 0.7, 0.8, 1.0, the 3D-J-aggregate orthorhombic model (*3D-40-mer*), i.e., β=90° and Delta=Slip=11.656 Å with other parameters being same as those of monoclinic model. In the *last four* frames, each bandshape is calculated respectively by uniformly scaling down, by the factor 0.6, 0.7, 0.8, 1.0, the 3D-J-aggregate monoclinic model [(*3D-40-mer*) with Delta=10.028 Å, Slip=13.080 Å. In the *first* and *eighth* frames, the same monomer bands of PIC molecule are plotted. In the backward frame, the monomer band and the J-split band of the PIC bromide are plotted from Ref. 8.

ing, by the factor 0.6, 0.7, 0.8, 1.0, the crystal model which is modified to be orthorhombic, i.e., β=90° and Delta=Slip=11.656 Å with other parameters being same. However, in the last four frames of Fig. 5, we plot the absorption bandshapes calculated respectively by scaling down the 3D-J-aggregate monoclinic crystal model (*3D-40-mer*) with Delta=10.028 Å, Slip=13.080 Å,[29] that is, by uniformly shortening the crystal structure by the factor 0.6, 0.7, 0.8, 1.0.

As seen in the three Figures, the *split* J-bands are not observed for the 1D-J-aggregate model. In Fig. 4, the 2D-J1- and 2D-J2-models with the shorter lattice constants, respectively, give rise to the *doubly* and/or *multiply* split J-bands. When we look at the most backward frame of Fig. 4, the 2D-J1-model scaled by the factor 0.9 appears to give the bandshape similar to the weak doublet J-band of PIC iodide observed,[5] while in the most forward frame, the 2D-J2-model scaled by the factor 0.6 seems to give the feature of the J-split band observed in the PIC bromide aggregate.[3,4,8]. However, the peak positions (563 and 572 nm) of J-split band by the factor 0.6 are insufficient to give a good agreement with the experimental values (571 and 577 nm). These doublet and/or multiplet structures obtained may be assigned to the Davydov splitting of J-band due to the interaction among 1D-J-aggregates, as suggested tacitly by Cooper.[3,4]

On the other hand, the unscaled orthorhombic 3D-J-model gives the single J-band as shown in the fourth frame of Fig. 5, but the orthorhombic model scaled by the factor 0.6 as shown in the most forward frame appears to give the split J-band with main two peaks (570 and 586 nm) separated by 430 cm^{-1}, which is compared with the split J-band of PIC bromide plotted in the most backward frame. However, we must note that the present orthorhombic model scaled by the factor 0.6 is not equal to the orthorhombic crystal model of PIC bromide.[27] It is noticed that as shown in the *eigth* frame of Fig. 5, the *unscaled monoclinic* crystal model PIC iodide is calculated to give the split J-band, i.e., the weak peak at 571 nm and the strong peak at 583 nm with a separation 360 cm^{-1}, which has a feature of J-split aggregate of PIC iodide.[5] It is to be noted that contrary to the unscaled orthorhombic 3D-J-model, the unscaled 1D-J-aggregate model which has the same geometrical parameters those of the crystal does not show a sharp J-band, as mentioned above.

From the monomer and the dimer spectra of PIC

molecule, Kopainsky el al.[17] estimated the essential parameters required also in the present calculations, for an example, the nearest neighbor electronic interaction which Knapp et al.[16] have applied to the bandshape calculations of linear J-aggregates ignoring non-nearest neighbor interactions. Different from Refs. 16 and 17 however, the calculations obtained indicate that the J-aggregate models assumed from the crystal structure do not necessarily have the same structure of essential dimer unit as Knapp et al. have assumed, in each process of aggregation in solution such as monomer→dimer→H-aggregate→J-aggregate.[10,29,30,32] The present calculations have revealed that the bandshapes are extremely sensitive to the geometrical values as well as the monomer spectroscopic parameters used. In case when the polymerization energy shift[16–18] appeared as Stokes shift is tentatively considered by changing $E_{fm,0}$ in Eqs. 1 and 4, the banshapes obtained are found to fall into the range of the present results. So before going a step further to consider the more exact formalism in order for cultivating a better understanding of unusual features of PIC aggregates, it is rather necessary to accumulate the numerical experiences about the geometries of PIC aggregate models, of course by making use of appropriate monomer spectroscopic data of PIC halides, in the belief that the real aggregate model in either solution or glassy solution is quite similar to the crystal structure. We need further studies to get a goal for predicting the whole feature of J-split bands, although the monoclinic 3D-J-four-inter-polymer model of PIC iodide leads to the qualitative feature of the doublet J-band as shown in the the *eighth* frame. For instance, the prediction for the two bands appeared at the shorter wavelength side of the split J-band in the *eighth* frame is failed. However, tentative calculations in the present formulation have been found to give some qualitative features in this region by increasingly piling up the PIC dimers and the columns of PIC's along the *y*-direction (*b*-axis) as shown in Fig. 2. Studies on such models are now in progress.

References

1) E. E. Jelley, *Nature,* **138**, 1009 (1936), *ibid.,* **139**, 631 (1937).
2) G. Scheibe, *Angew. Chem.,* **49**, 563 (1936).
3) W. Cooper, *Chem. Phys. Lett.,* **7**, 73 (1970).
4) W. Cooper, *Photogr. Sci. Eng.,* **17**, 217 (1973).
5) J. Tanaka, M. Tanaka, and M. Hayakawa, *Bull. Chem. Soc. Jpn.,* **53**, 3109 (1980).
6) A. P. Marchetti, C. D. Salzberg, and E. I. P. Walker, *Photogr. Sci. Eng.,* **20**, 107 (1976).
7) A. P. Marchetti, C. D. Salzberg, and E. I. P. Walker, *J. Chem. Phys.,* **64**, 4693 (1976).
8) Z. X. YU, P. Y. Lu, and R. R. Affano, *Chem. Phys.,* **79**, 289 (1983).
9) R. Hirschmann, W. Koler, J. Friedrich, and E. Daltrozzo, *Chem. Phys. Lett.,* **151**, 60 (1988).
10) M. Murata, *J. Soc. Photogr. Sci. Technol. Jpn.,* **52**, 24 (1989).
11) A. Herzenberg and A. Modinos, *Proc. R. Soc.,* **87**, 597 (1966).
12) H. Ito and Y. J. I'Haya, *J. Chem. Phys.,* **77**, 6270 (1982).
13) J. S. Briggs and A. Herzenberg, *Mol. Phys.,* **21**, 865 (1971).
14) J. S. Briggs and A. Herzenberg, *Mol. Phys.,* **23**, 203 (1972).
15) H. Sumi, *J. Phys. Soc. Jpn.,* **38**, 825 (1975).
16) E. W. Knapp, P. O. J. Scherer, and S. F. Fischer, *Chem. Phys. Lett.,* **111**, 481 (1981).
17) B. Kopainsky, J. K. Hallermeier, and W. Kaiser, *Chem. Phys. Lett.,* **83**, 498 (1981).
18) P. O. J. Scherer and S. F. Fischer, *Chem. Phys.,* **86**, 269 (1984).
19) H. Ito and Y. J. I'Haya, *Bull. Chem. Soc. Jpn.,* **60**, 2791 (1987).
20) H. Ito, T. Eri, and Y. J. I'Haya, *Chem. Phys.,* **8**, 68 (1975); *ibid.,* **10**, 49715 (1975).
21) A. V. Lukashin and M. D. Frank-Kamenetskii, *Chem. Phys. Lett.,* **45**, 36 (1977).
22) F. K. Fong, "Radiationless Processes in Molecules and Condensed Phases," Springer-Verlag, Berlin (1976), p. 4.
23) R. P. Hemenger, *J. Chem. Phys.,* **67**, 262 (1977).
24) H. Ito and Y. J. I'Haya, *Chem. Phys. Lett.,* **142**, 25 (1987).
25) A. V. Lukashin and M. D. Frank-Kamenetskii, *Chem. Phys. Lett.,* **45**, 36 (1977).
26) B. J. Caldwell and H. Eyring, "The Theory of Optical Activity," Wiley-Interscience, New York (1971), p. 77.
27) V. B. Dammeier and W. Hoppe, *Acta Crystallogr., Sect. B,* **27**, 2364 (1971).
28) H. Yoshioka and K. Nakatsu, *Chem. Phys. Lett.,* **11**, 255 (1971).
29) K. Nakatsu, H. Yoshioka, and H. Morishita, *Acta Crystallogr., Sect. B,* **33**, 2181 (1977).
30) E. Daltrozzo, G. Scheibe, K. Gschwind, and F. Haimerl, *Photogr. Sci. Eng.,* **18**, 441 (1974).
31) R. L. Ellis, G. Kuehnlenz, and H. H. Jaffe', *Theor. Chim. Acta (Berlin),* **26**, 131 (1972).
32) A. H. Hertz, *Photogr. Sci. Eng.,* **18**, 323 (1974).
33) D. L. Smith, *Photogr. Sci. Eng.,* **18**, 309 (1974).
34) H. Kuhn, *J. Chem. Phys.,* **53**, 101 (1970).